

Topologically non-trivial magnon bands in artificial square spin ices subject to Dzyaloshinskii-Moriya interaction

Ezio Iacocca^{1,2,*} and Olle Heinonen^{3,4}

¹*Department of Applied Mathematics, University of Colorado, Boulder, Colorado 80309-0526, USA*

²*Department of Physics, Division for Theoretical Physics,
Chalmers University of Technology, 412 96, Gothenburg, Sweden*

³*Materials Science Division, Argonne National Laboratory, Lemont, IL 60439, USA*

⁴*Northwestern-Argonne Institute for Science and Engineering, Evanston, IL 60208, USA*

Systems that exhibit topologically protected edge states are interesting both from a fundamental point of view as well as for potential applications, the latter because of the absence of back-scattering and robustness to perturbations. It is desirable to be able to control and manipulate such edge states. Here, we demonstrate using a semi-analytical model that artificial square ices can incorporate both features: an interfacial Dzyaloshinskii-Moriya gives rise to topologically non-trivial magnon bands, and the equilibrium state of the spin ice is reconfigurable with different states having different magnon dispersions and topology. Micromagnetic simulations are used to determine the magnetization equilibrium states and to validate the semi-analytical model. Our results are amenable to experimental verification via, e.g., lithographic patterning and micro-focused Brillouin light scattering.

I. INTRODUCTION

Topological insulators¹⁻⁶ are generally materials that are insulating in the bulk but have conducting dissipationless edge states⁷. In two dimensions, topological insulators include quantum Hall (QH) states^{8,9}. QH edge states are metallic and chiral in that edge states on one physical edge move only in one direction; this prohibits back-scattering and makes the states dissipationless. The existence of topologically protected edge states is guaranteed if the band structure of the system has a non-trivial topology. A non-trivial topology is characterized by a non-zero Chern number, which is related to the Berry's phase that Bloch states $|u_{n,\vec{k}}\rangle$, where \vec{k} is a wavevector in the first Brillouin zone and n a band index, acquire when transported around a closed loop in the Brillouin zone; the Chern number is the total flux of the Berry's phase in the Brillouin zone. Therefore, in order for there to be a non-trivial topology, the Berry's phase accumulated around a closed loop cannot be zero. This may happen, but is not assured, if time-reversal invariance is broken.

Topologically protected dissipationless edge states are obviously of great interest for potential applications, for example in information technology or communications systems. This extends beyond electronic systems, such as photonic TIs^{10,11} and magnonic TIs^{12,13}. In these latter system, the band structure of spin excitations, or magnons, exhibit a topological order with non-trivial Chern number and protected edge states, in the sense that they cannot backscatter. However, systems with potential practical applications should be reconfigurable, so that the band structure of excitations can be modified with some external control parameter.

Artificial spin ices (ASIs)¹⁴⁻¹⁶ are systems that allow for such reconfiguration. ASIs are composed of geometrically placed magnetic nanoislands coupled through dipolar interactions. These interactions stabilize the nanois-

lands' magnetization in configurations such that the magnetization at the lattice vertices satisfy an "ice rule" in low-energy states. ASIs are geometrically frustrated by design, that is, not all interactions at a given vertex can be simultaneously minimized. This leads to complex energy surfaces with many local energy minima. Consequently, significant efforts have been devoted to control and manipulate the magnetization state either by thermal or applied field protocols¹⁷ or novel geometries¹⁸. This makes ASIs a natural system in which to explore reconfigurable magnonics, where the properties of the spin wave band structure can be actively controlled¹⁹⁻²⁴.

An initial study by Gliga et al.¹⁹ suggested that the magnon modes of square ASIs, where the magnetic nanoislands are placed at the sites of a square lattice, are modified by the existence of underlying defects known as Dirac strings¹⁶. These defects originate as the ice rule is locally broken, yet conserving the overall topological charge of the system. More recent works have numerically²¹ and experimentally²² shown that the square ASI magnetization ground state determines the features and eigenfrequencies of the magnon modes.

These ASIs, though reconfigurable magnonic crystals, have magnon band structures with trivial topologies. It is of great interest to devise magnonic crystals that have non-trivial topological order *and* that are reconfigurable. One way to realize such systems is to introduce interfacial Dzyaloshinskii-Moriya interactions (DMI)^{25,26} to ASIs. DMI generally arises in three-dimensional systems with broken inversion symmetry and allows for a chiral magnetic interaction that can give rise to topological spin textures such as skyrmions²⁷⁻²⁹. More conveniently, an interfacial DMI can arise when a trivial magnet, such as Permalloy or CoFeB, is deposited as a thin film on a strong spin-orbit scatterer, such as Ta or Pt. This effect has been used experimentally²⁸ and numerically²⁹⁻³¹ to nucleate and dynamically drive skyrmions at room temperature. Interfacial DMI naturally has a thickness-

dependent strength³², parametrized by an interfacial energy D in units of J/m^2 . Although most of the research on DMI has focused on topological structures or non-reciprocal spin wave dispersion in extended films^{32,33}, the effect of DMI for spin waves in magnetic nanoislands has been studied only recently³⁴. In the context of magnonic square ASIs, the addition of a chiral interfacial DMI suggests the possibility of topological magnon modes and novel features in their band structure. The purpose of our work is to demonstrate, using micromagnetic and semi-analytical models, that interfacial DMI in a square ASI can give rise to a topologically non-trivial magnon band structure, analogous to an electronic TI. In a magnonic system without DMI, the magnons are elliptical revolutions of the magnetization about its local equilibrium direction, and modes at $(\pm\mathbf{k}, n)$ are degenerate. The form of the interfacial DMI breaks this degeneracy³⁴ as it gives rise to an effective magnetic field

$$\vec{H}_{\text{DMI}} = \frac{2D}{M_s} [(\nabla \cdot \vec{m}) \hat{z} - \nabla m_z] \quad (1)$$

that couples differently to states at \vec{k} and $-\vec{k}$. We will show that there is a thickness-dependent critical coupling D_c , at which non-trivial topologies emerge. Furthermore, by reconfiguring the equilibrium state of the lattice from a vortex state to a remanent state, the non-trivial topology can be turned off.

II. SEMI-ANALYTICAL MODEL

The band structure of a square ASIs can be computed, to good approximation, by a semi-analytical model²¹ based on small-amplitude perturbations of the Larmor equation

$$\frac{\partial \vec{m}}{\partial t} = -\gamma \mu_0 \vec{m} \times \vec{H}_{\text{eff}}, \quad (2)$$

where γ is the gyromagnetic ratio, μ_0 is the vacuum permeability, \vec{m} is the magnetization vector normalized to the saturation magnetization M_s , and \vec{H}_{eff} is the effective field, including contributions from external magnetic fields, exchange, anisotropy, dipolar inter-island coupling, and DMI. Performing a Holstein-Primakoff transformation and expanding about a well-defined magnetization state, it is possible to rewrite Eq. (2) as a Hamiltonian equation in terms of complex amplitudes³⁵. The resulting Hamiltonian model can be generalized for $2n$ interacting complex amplitudes and their complex conjugates and expressed as an eigenvalue problem by means of Colpa's grand dynamical matrix³⁶

$$\omega \underline{\psi} = \mathcal{H} \underline{\psi} = \begin{pmatrix} \mathcal{H}^{(1,2)} & \mathcal{H}^{(2,2)} \\ \mathcal{H}^{(1,1)} & \mathcal{H}^{(2,1)} \end{pmatrix} \underline{\psi}, \quad (3)$$

from which we obtain the eigenvalues ω and eigenvectors $\underline{\psi}$. Because of the periodic structure of the ASI, we can

label the eigenvectors $\underline{\psi}$ by a wvector \vec{k} in the first Brillouin zone, and a band index n . The Hamiltonian matrix \mathcal{H} is related to the effective field via $\mathcal{H} = -\gamma \delta W / (2M_s)$, where $\delta W = -\int \vec{H}(\vec{M}) \cdot d\vec{M}$ is the energy functional. In Ref. 21, the Hamiltonian matrices for an external in-plane field as well as anisotropy, dipole-dipole, and exchange fields were derived. Notably, the exchange field contribution was found to be critical to correctly describe the band diagram due to the bent magnetization at the nanoislands' edges²⁰. Because we are interested in the low-energy sector of the square ASI dynamics, the magnetic nanoislands are divided in $\mathcal{N} = 3$ macrospins coupled by an effective exchange strength. Good agreement with micromagnetic simulations further confirmed this approach²¹.

Here, we extend the model to include DMI, which means we have to include the effective interfacial DMI field²⁹, given by Eq. (1). This field favors a chiral tilt of the perpendicular magnetization component that stabilizes helical order in extended films³⁷. Therefore, the model must consider small-amplitude precession in all three magnetization components. The resulting Hamiltonian matrices for the effective interfacial DMI field are

$$\mathcal{H}_{\text{DMI}}^{(1,1)} = D' \begin{pmatrix} V_1 & \mathcal{O} & \mathcal{O} & \mathcal{O} \\ \mathcal{O} & H_1 & \mathcal{O} & \mathcal{O} \\ \mathcal{O} & \mathcal{O} & V_1 & \mathcal{O} \\ \mathcal{O} & \mathcal{O} & \mathcal{O} & H_1 \end{pmatrix} \quad (4a)$$

$$\mathcal{H}_{\text{DMI}}^{(1,2)} = D' \begin{pmatrix} V_2 & \mathcal{O} & \mathcal{O} & \mathcal{O} \\ \mathcal{O} & H_2 & \mathcal{O} & \mathcal{O} \\ \mathcal{O} & \mathcal{O} & V_2 & \mathcal{O} \\ \mathcal{O} & \mathcal{O} & \mathcal{O} & H_2 \end{pmatrix}, \quad (4b)$$

where $V_1^{i,j}$, $V_2^{i,j}$, $H_1^{i,j}$, and $H_2^{i,j}$ are $\mathcal{N} \times \mathcal{N}$ complex matrices relating the intra-island magnetization components, given in the appendix, and \mathcal{O} are $\mathcal{N} \times \mathcal{N}$ zero matrices. The effective DMI parameter in our discrete, macrospin representation is given by

$$D' = \frac{\gamma D}{2M_s t}, \quad (5)$$

where the inverse dependence on thickness reflects the interfacial nature of this effect. However, we stress that the field Eq. (1) is considered to be homogeneous across the thickness; this is a good approximation for thin islands in which the magnetization at any point is uniform through the thickness.

Because the semi-analytical method relies on a second-order perturbation of a well-defined magnetization state, the effect of DMI can only be included as a deviation from such a state i.e., low DMI strengths. The initial equilibrium states are determined by energy minimization using Eq. (2) with an added Gilbert damping term, which we calculate from full-scale micromagnetic simulations as detailed below.

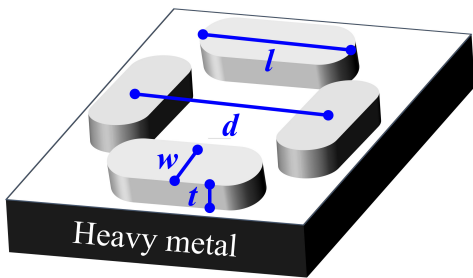


FIG. 1. (color online) Schematic of the square ASI unit cell. The composing nanoislands are identical with length l , width w , and thickness t . The lattice constant d is taken as the center-to-center distance between adjacent nanoislands. Interfacial DMI is imparted through a heavy metal layer.

III. CHERN NUMBER

The introduction of DMI in a square ASI breaks time-reversal invariance which suggests that topological modes may exist. To test for topology, we calculate the Chern number C_n for band n , defined as

$$C_n = \frac{1}{2\pi i} \int \left(\partial_x A_y(\vec{k}) - \partial_y A_x(\vec{k}) \right) d^2k \quad (6)$$

where $A_\mu = \langle \underline{\psi}(k), \partial_\mu \underline{\psi}(k) \rangle$ is the Berry connection, $\mu = x, y$, and the eigenmodes $\underline{\psi}$ belong to band n . A non-zero Chern number indicates that the band experiences inversion which, in a finite lattice, leads to topological edge modes. We stress that the total Chern number of the band structure, obtained by summing C_n over the bands n , is conserved to zero. Thus any non-zero Chern number must be balanced with an opposite-signed Chern number.

The numerical computation of the Chern number is performed following the method given in Ref. 38. This method relies on lattice gauge theory to calculate the Chern number in a discretized Brillouin zone regardless of the discretization in reciprocal space.

IV. MICROMAGNETIC SIMULATIONS

The equilibrium configurations of square ASIs subject to interfacial DMI are determined by micromagnetic simulations. We use the GPU-accelerated software Mumax3³⁹. The square ASI unit cell and geometry is schematically shown in Fig. 1, with lattice constant $d = 390$ nm. The nanoisland are considered to be identical, with lateral dimensions $l = 290$ nm and $w = 130$ nm, thickness series $t = 10, 15,$ and 20 nm, $M_s = 800$ A/m, and exchange stiffness $A = 13$ pJ/m. The magnetic parameters were chosen to be consistent with bulk Py or a similar NiFe composition. We consider a heavy metal layer below the square ASI, that endows the ferromagnetic nanoislands with an interfacial DMI. Numerically, we solve for a square ASI unit cell and impose periodic

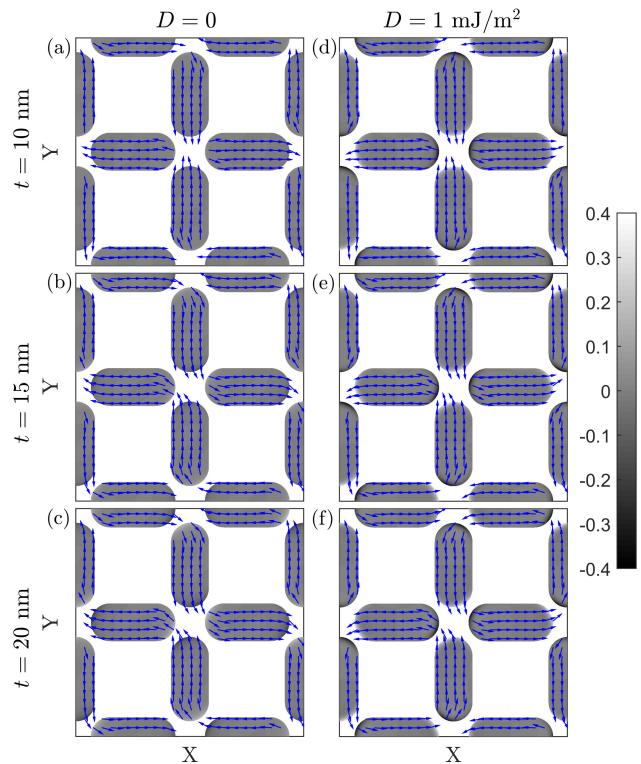


FIG. 2. (color online) Ground states for a series of nanoislands' thicknesses with (a-c) $D = 0$ and (d-f) $D = 1$ mJ/m² obtained by micromagnetic simulations. The gray scale (arrows) represents the \hat{z} magnetization component (in-plane magnetization component). The S-states at $D = 0$ are observed to transition to C-states for $D \approx 1$ mJ/m².

boundary conditions to simulate an extended lattice. To correctly account for the nanoislands' round edges in the micromagnetic finite difference scheme, we use a rather small cell size of 0.7 nm in-plane and 5 nm along the thickness⁴⁰.

Two equilibrium configurations are computed: the remanent and vortex states. The simulation is initialized by setting a homogeneous magnetization in each nanoisland composing either of these states and allowing the simulation to relax using an artificially high Gilbert damping constant $\alpha = 1$. In the remanent state, the equilibrium configurations are S-states and they are insensitive to DMI strength. In contrast, the vortex state exhibits a richer behavior as a function of D . For $D = 0$, S-states are obtained, as shown in Fig. 2(a-c) for the considered thickness series, where grayscale (arrow) represents the \hat{z} (in-plane) magnetization component of the topmost layer. The inclusion of DMI favors C-states for all thicknesses, as shown for $D = 1$ mJ/m² in Fig. 2(d-f). Additionally, the DMI contributes to an out-of-plane tilt of the magnetization at the nanoislands' edges that is odd along the length of the island. However, this tilt is small and does not contribute significantly to the band structure. These simulations confirm that a moderate DMI only slightly perturbs the stable magnetiza-

tion state in a square ASI, making it possible to study the full band structure by the semi-analytical model and exhibits different behavior for underlying magnetic equilibrium configurations. We note that labyrinthine, chiral magnetization states are obtained for all thicknesses when $D \geq 3$ mJ/m².

The spectrum at the Γ point can be obtained micro-magnetically by analyzing the equilibration after a weak perturbation of the system. We use a spatially homogeneous square field pulse as perturbation, with a duration of 50 ps and a field magnitude of 10 mT applied along the (1, 1) direction. The system is then relaxed for 10 ns using a Gilbert damping of $\alpha = 0.01$. This method only couples the uniform field to even modes. In the remanent state, constant eigenfrequencies are obtained as a function of D , as expected from the negligible impact of DMI on the equilibrium configuration. These eigenfrequencies are in agreement with those observed in Ref. 21 and are thus topologically trivial, which we confirmed by calculating the Chern numbers of the magnon bands. In the vortex state, the D -dependent eigenfrequencies are shown in Fig. 3 for each thickness by red circles (bulk mode) and asterisks (low-frequency edge modes). We note as a trend that the frequency drops as a function of D , consistent with the lower frequencies in the band diagram obtained from a C-state relative to an S-state²¹. It is also important to recognize that whereas we observe a single, fundamental bulk mode, the edge mode frequencies are split, consistent with the spin wave non-reciprocity induced by DMI and evidenced by a shift in their dispersion relation³². However, we note that the frequency splitting is small and cannot be accurately determined within our numerical resolution of 24.5 MHz.

V. SEMI-ANALYTICAL RESULTS

Motivated by the micromagnetic simulations, we now utilize the semi-analytical model to solve for the eigenvalues in a square ASI with variable thickness and DMI. First, we validate the semi-analytical model by finding the eigenvalues at the Γ point as a function of D in the vortex state. The magnetization vector for each macrospin is estimated from the spatial average of the micromagnetic magnetization equilibrium configuration. In order to describe the transition from an S- to a C-state, we fit the magnetization vector obtained with $D = 0, 0.5, \text{ and } 1$ mJ/m². A quadratic function is found to be sufficient to capture the transition. Utilizing the out-of-plane anisotropy factor as the only fitting parameter (approximated to first order from an ellipsoid⁴¹), we fit the frequency of the even bulk mode. Without any other fitting parameters, we observe good agreement between the semi-analytical (solid blue line) and micromagnetic (red circles) bulk mode frequency dependence on D up to 0.75 mJ/m² for all thicknesses, Fig. 3. Higher values for D strongly perturb the equilibrium state and dynamics of the nanoislands at a length scale much smaller than that

captured by the three macrospins considered in the semi-analytical model. The lowest even edge mode frequency approximately agrees in magnitude, but strong oscillations are obtained from the semi-analytical model (black dashed line) as a function of D in contrast to weak oscillations observed from micromagnetics (red asterisks). The strong oscillations in the semi-analytical model are attributed to the transition between S- and C-states that is captured only approximately by the three-spin model of each island. Consequently, the off-diagonal Hamiltonian matrix, Eq. (4a), can become exactly zero so that the frequency shift due to DMI is directly given by the diagonal Hamiltonian matrix components Eq. (4b). This occurs at the oscillation maxima. In contrast, the large number of cells used in the micromagnetic simulations ensures a smooth S- to C-transition so that the off-diagonal terms will not cancel, minimizing the oscillations. However, the mechanism responsible for the larger oscillations in the semi-analytical model does not affect the topology of the band structure as it gives rise to a trivial shift in energy at the Γ point.

The observed agreements suggest that the semi-analytical model captures the relevant physics to describe the band diagram of square ASIs, including interfacial DMI. It is worth noting that the semi-analytical model returns a total of twelve bands with three even- and nine odd-symmetry modes. As mentioned before, odd-symmetry modes cannot be excited micromagnetically with a homogeneous field; therefore, the semi-analytically-obtained odd modes are not shown in Fig. 3. Notably, as we show below, topological modes exist precisely in these odd modes.

We now calculate the band structure in the first Brillouin zone in the vortex state. For each band n , the Chern number C_n can be calculated by the method out-

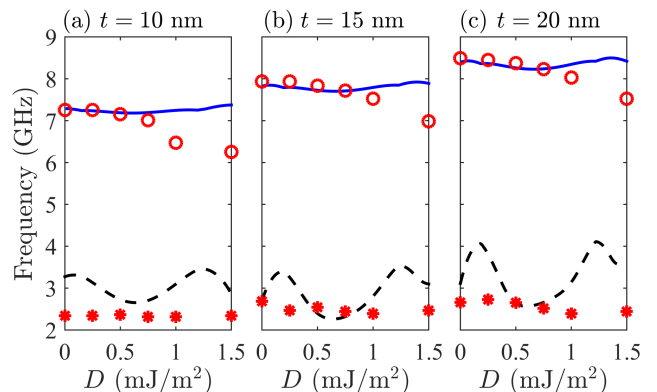


FIG. 3. (Color online) Even-mode frequencies at the Γ point as a function of D for nanoislands of thickness (a) 10, (b) 15, and (c) 20 nm. Good agreement is observed between the semi-analytical (solid blue line) and micromagnetic (red circles) bulk mode. The lowest-energy modes obtained with the semi-analytical mode (black dashed line) exhibits oscillations as a function of D which are much more pronounced than obtained from micromagnetics (red asterisks) (see text).

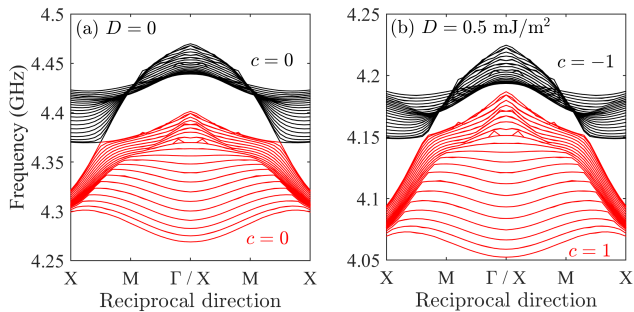


FIG. 4. (color online) Projection of the odd edge mode bands with (a) $D = 0$, $c = 0$ and (b) $D = 0.5 \text{ mJ/m}^2$, $c = \pm 1$ for nanoislands of $t = 10 \text{ nm}$. Nonzero Chern numbers are related to constructive action of Berry phases arising at the Dirac cones observed along the Γ -X direction in (b).

lined in Sec. III. When $D = 0$ we find $c = 0$ for all thicknesses. However, for a thickness-dependent critical $D_c(t) \neq 0$, we find nonzero Chern numbers for the odd-symmetry edge modes. As an example, we show the projection of the bands exhibiting trivial ($D = 0$) and finite ($D = 0.5 \text{ mJ/m}^2$) topological features in Fig. 4(a) and (b), respectively, for a thickness $t = 10 \text{ nm}$. The value $D = 0.5 \text{ mJ/m}^2$ is chosen on the basis of best agreement between the eigenfrequencies at the Γ point obtained micromagnetically and semi-analytically, see Fig. 3. Interestingly, we observe bands coalescing in a single point along the Γ -X direction. In the case $D = 0$, a trivial topology is maintained as the bands cross without inversion, as observed in Ref. 21. In terms of the Chern number, this implies that the band crossings contribute with non-zero Berry phases that cancel each other, leading to a net trivial topology. In contrast, for $D = 0.5 \text{ mJ/m}^2$, the bands touch in Dirac cones and exhibit inversion which, from a topological perspective, indicates constructive Berry phases and a non-zero Chern number. Note that, as expected, the bands shown in Fig. 4(b) have oppositely signed Chern numbers, maintaining the overall topology (sum of the Chern numbers) of zero. The same behavior is obtained for larger values of D , suggesting that a non-zero topology for odd modes is a robust feature of the band structure, regardless of the discretization effects on the quantitative eigenfrequencies. In stark contrast, the band diagram for the remanent state is topologically trivial as a function of D . This implies that it is possible to toggle between topological edge and non-topological modes in a square ASIs by configuring the underlying magnetization configuration.

The critical DMI strength for non-zero Chern numbers can be numerically estimated as a function of thickness making use of the interpretation provided above. We find $D_c(10) = 0.22$, $D_c(15) = 0.28$, and $D_c(20) = 0.1 \text{ mJ/m}^2$, with thicknesses in the parentheses given in nm and with an error of $\pm 0.03 \text{ mJ/m}^2$. Counterintuitively, we find that D_c sharply decreases at $t = 20 \text{ nm}$, where the DMI effect should be minimized. This is associated to the

breakdown of the semi-analytical model that does not incorporate a discretization across the nanoisland thickness and therefore the DMI, although weak, is uniform. Physically, interfacial DMI in thick nanoislands will feature a competition between DMI-induced and DMI-free layers, diminishing the overall effect of DMI on the band structure of the square ASI.

VI. CONCLUSIONS

In summary, we have calculated the spin wave band structure for square ASIs taking into account interfacial DMI imparted, e.g., by an adjacent heavy metal layer. The chiral nature of the DMI influences the eigenmodes supported by the square ASI, leading to band inversion through the development of Dirac cones. This suggests that DMI can support topologically protected modes at the edges of finite square ASIs. Only odd-symmetry magnon bands that arise from coupled magnetization oscillations at the edges of the islands develop topologically non-trivial states. This is consistent with the fact that these modes can more efficiently couple with neighboring spins whereas their odd symmetry reflects the non-reciprocal nature of long-range spin waves under the influence of interfacial DMI. Our findings constitute an experimental approach to impart, tune, and verify topological features in square ASIs. For example, micro-focused Brillouin light scattering experiments⁴² can determine the existence of topologically protected edge modes in square ASIs as a function of the spin-orbit scatterer material and the thickness of the magnetic material. Furthermore, these features can be reconfigured and the non-trivial band topology – and concomitantly topologically protected edge states – turn off by changing the underlying magnetization configuration of the square ice, i.e., by different field protocols²² to relax the nanoislands' magnetization.

ACKNOWLEDGMENTS

E. I. acknowledges support from the Swedish Research Council, Reg. No. 637-2014-6863. The work by O. H. was funded by the Department of Energy Office of Science, Materials Sciences and Engineering Division. We gratefully acknowledge the computing resources provided on Blues, a high-performance computing cluster operated by the Laboratory Computing Resource Center at Argonne National Laboratory.

Appendix A: Matrix components of the DMI Hamiltonian

The Hamiltonian matrices are written in terms of the complex amplitudes a , which are related to the normalized magnetization vector through their spherical com-

ponents i.e., the polar and azimuthal angles θ and φ (See Ref. 35 and Ref. 21 for details). By performing the cross product $\vec{m}_i \times \vec{m}_j$, where i and j are two neighboring macrospins in a nanoisland, and keeping terms to second order in a , we obtain the $\mathcal{N} \times \mathcal{N}$ matrices

$$V_1 = \begin{pmatrix} 0 & R_v^{1,2} & 0 \\ R_v^{2,1} & 0 & R_v^{2,3} \\ 0 & R_v^{3,2} & 0 \end{pmatrix}, \quad (\text{A1a})$$

$$V_2 = \begin{pmatrix} S_v^{1,2} + S_v^{2,1} & C_v^{1,2} & 0 \\ C_v^{2,1} & \sum S_v & C_v^{2,3} \\ 0 & C_v^{3,2} & S_v^{2,3} + S_v^{3,2} \end{pmatrix}, \quad (\text{A1b})$$

$$H_1 = \begin{pmatrix} 0 & R_h^{1,2} & 0 \\ R_h^{2,1} & 0 & R_h^{2,3} \\ 0 & R_h^{3,2} & 0 \end{pmatrix}, \quad (\text{A1c})$$

$$H_2 = \begin{pmatrix} S_h^{1,2} + S_h^{2,1} & C_h^{1,2} & 0 \\ C_h^{2,1} & \sum S_h & C_h^{2,3} \\ 0 & C_h^{3,2} & S_h^{2,3} + S_h^{3,2} \end{pmatrix}, \quad (\text{A1d})$$

where $\sum S_v = S_v^{1,2} + S_v^{2,1} + S_v^{2,3} + S_v^{3,2}$, $\sum S_h = S_h^{1,2} + S_h^{2,1} + S_h^{2,3} + S_h^{3,2}$, and

$$R_v^{i,j} = \sin \theta_i \sin \varphi_i \cos \theta_j - \sin \theta_j \sin \varphi_j \cos \theta_i + i (|\cos \varphi_j| \cos \theta_i - |\cos \varphi_i| \cos \theta_j) \quad (\text{A2a})$$

$$S_v^{i,j} = 2 (\cos \theta_j \sin \varphi_j \sin \theta_i - \cos \theta_i \sin \varphi_i \sin \theta_j) \quad (\text{A2b})$$

$$C_v^{i,j} = \sin \theta_j \sin \varphi_j \cos \theta_i - \sin \theta_i \sin \varphi_i \cos \theta_j + i (|\cos \varphi_i| \cos \theta_j + |\cos \varphi_j| \cos \theta_i) \quad (\text{A2c})$$

$$R_h^{i,j} = \sin \theta_i \cos \varphi_i \cos \theta_j - \sin \theta_j \cos \varphi_j \cos \theta_i + i (|\sin \varphi_j| \cos \theta_i - |\sin \varphi_i| \cos \theta_j) \quad (\text{A2d})$$

$$S_h^{i,j} = 2 (\cos \theta_j \cos \varphi_j \sin \theta_i - \cos \theta_i \cos \varphi_i \sin \theta_j) \quad (\text{A2e})$$

$$C_h^{i,j} = \sin \theta_j \cos \varphi_j \cos \theta_i - \sin \theta_i \cos \varphi_i \cos \theta_j + i (|\sin \varphi_i| \cos \theta_j + |\sin \varphi_j| \cos \theta_i) \quad (\text{A2f})$$

$$(\text{A2g})$$

-
- * ezio.iacocca@colorado.edu
- ¹ J. E. Moore and L. Balents, *Physical Review B* **75**, 121306 (2007).
 - ² D. Hsieh, D. Qian, L. Wray, Y. Xia, Y. S. Hor, R. Cava, and M. Z. Hasan, *Nature* **452**, 970 (2008).
 - ³ D. Hsieh, Y. Xia, D. Qian, L. Wray, J. Dil, F. Meier, J. Osterwalder, L. Patthey, J. Checkelsky, N. Ong, *et al.*, *Nature* **460**, 1101 (2009).
 - ⁴ Y. Xia, D. Qian, D. Hsieh, L. Wray, A. Pal, H. Lin, A. Bansil, D. Grauer, Y. Hor, R. Cava, *et al.*, *Nature Physics* **5**, 398 (2009).
 - ⁵ D. Hsieh, Y. Xia, L. Wray, D. Qian, A. Pal, J. Dil, J. Osterwalder, F. Meier, G. Bihlmayer, C. Kane, *et al.*, *Science* **323**, 919 (2009).
 - ⁶ M. Z. Hasan and C. L. Kane, *Reviews of Modern Physics* **82**, 3045 (2010).
 - ⁷ P. Roushan, J. Seo, C. V. Parker, Y. Hor, D. Hsieh, D. Qian, A. Richardella, M. Z. Hasan, R. Cava, and A. Yazdani, *Nature* **460**, 1106 (2009).
 - ⁸ D. Thouless, M. Kohmoto, M. Nightingale, and M. Den Nijs, *Physical Review Letters* **49**, 405 (1982).
 - ⁹ Q. Niu, D. J. Thouless, and Y.-S. Wu, *Physical Review B* **31**, 3372 (1985).
 - ¹⁰ A. B. Khanikaev, S. H. Mousavi, W.-K. Tse, M. Kargarian, A. H. MacDonald, and G. Shvets, *Nature materials* **12**, 233 (2013).
 - ¹¹ M. C. Rechtsman, J. M. Zeuner, Y. Plotnik, Y. Lumer, D. Podolsky, F. Dreisow, S. Nolte, M. Segev, and A. Szameit, *Nature* **496**, 196 (2013).
 - ¹² R. Shindou, R. Matsumoto, S. Murakami, and J.-i. Ohe, *Phys. Rev. B* **87**, 174427 (2013).
 - ¹³ R. Shindou, J.-i. Ohe, R. Matsumoto, S. Murakami, and E. Saitoh, *Phys. Rev. B* **87**, 174402 (2013).
 - ¹⁴ R. Wang, C. Nisoli, R. Freitas, J. Li, W. McConville, B. Cooley, M. Lund, N. Samarth, C. Leighton, V. Crespi, and P. Schiffer, *Nature* **439**, 303 (2005).
 - ¹⁵ C. Nisoli, R. Moessner, and P. Schiffer, *Rev. Mod. Phys.* **85**, 1473 (2013).
 - ¹⁶ L. J. Heyderman and R. L. Stamps, *Journal of Physics: Condensed Matter* **25**, 363201 (2013).
 - ¹⁷ A. Farhan, P. M. Derlet, A. Kleibert, A. Balan, R. V. Chopdekar, M. Wyss, J. Perron, A. Scholl, F. Nolting, and L. J. Heyderman, *Phys. Rev. Lett.* **111**, 057204 (2013).
 - ¹⁸ Y.-L. Wang, Z.-L. Xiao, A. Snezhko, J. Xu, L. E. Ocola, R. Divan, J. E. Pearson, G. W. Crabtree, and W.-K. Kwok, *Science* **352**, 962 (2016).
 - ¹⁹ S. Gliga, A. Kákay, R. Hertel, and O. G. Heinonen, *Phys. Rev. Lett.* **110**, 117205 (2013).
 - ²⁰ S. Gliga, A. Kákay, L. J. Heyderman, R. Hertel, and O. G. Heinonen, *Phys. Rev. B* **92**, 060413 (2015).
 - ²¹ E. Iacocca, S. Gliga, R. L. Stamps, and O. Heinonen, *Phys. Rev. B* **93**, 134420 (2016).
 - ²² M. B. Jungfleisch, W. Zhang, E. Iacocca, J. Sklenar, J. Ding, W. Jiang, S. Zhang, J. E. Pearson, V. Novosad, J. B. Ketterson, O. Heinonen, and A. Hoffmann, *Phys. Rev. B* **93**, 100401 (2016).
 - ²³ V. S. Bhat, F. Heimbach, I. Stasinopoulos, and D. Grundler, *Phys. Rev. B* **93**, 140401 (2016).
 - ²⁴ X. Zhou, G.-L. Chua, N. Singh, and A. O. Adeyeye, *Adv. Func. Mater.* (2016), 10.1002/adfm.201505165.
 - ²⁵ I. Dzyaloshinskii, *Journal of Physics and Chemistry of Solids* **4**, 241 (1958).
 - ²⁶ T. Moriya, *Phys. Rev.* **120**, 91 (1960).
 - ²⁷ U. Rössler, A. Bogdanov, and C. Pfeleiderer, *Nature* **442**, 797 (2006).
 - ²⁸ W. Jiang, P. Upadhyaya, W. Zhang, G. Yu, M. B. Jungfleisch, F. Y. Fradin, J. E. Pearson, Y. Tserkovnyak, K. L. Wang, O. Heinonen, S. G. E. te Velthuis, and A. Hoffmann, *Science* **349**, 283 (2015).
 - ²⁹ O. Heinonen, W. Jiang, H. Somaily, S. G. E. te Velthuis, and A. Hoffmann, *Phys. Rev. B* **93**, 094407 (2016).
 - ³⁰ J. Sampaio, V. Cros, S. Rohart, A. Thiaville, and A. Fert, *Nature Nanotechnology* **8**, 839 (2013).
 - ³¹ Y. Zhou, E. Iacocca, A. Awad, R. Dumas, H. Zhang, H. B. Braun, and J. Åkerman, *Nature Communications* **6** (2015).

- ³² H. T. Nembach, J. M. Shaw, M. Weller, E. Jué, and T. J. Silva, *Nature Physics* **11**, 825 (2015).
- ³³ F. Garcia-Sanchez, P. Borys, A. Vansteenkiste, J.-V. Kim, and R. L. Stamps, *Phys. Rev. B* **89**, 224408 (2014).
- ³⁴ B. W. Zingsem, M. Farle, R. L. Stamps, and R. E. Camley, arXiv:1609.03417 (2016).
- ³⁵ A. Slavin and V. Tiberkevich, *Magnetics*, *IEEE Transactions on* **45**, 1875 (2009).
- ³⁶ J. Colpa, *Physica A: Statistical Mechanics and its Applications* **93**, 327 (1978).
- ³⁷ M. Uchida, Y. Onose, Y. Matsui, and Y. Tokura, *Science* **20**, 359 (2006).
- ³⁸ T. Fukui, Y. Hatsugai, and H. Suzuki, *Journal of the Physical Society of Japan* **74**, 1674 (2005).
- ³⁹ A. Vansteenkiste, J. Leliaert, M. Dvornik, M. Helsen, F. Garcia-Sanchez, and B. Van Waeyenberge, *AIP Advances* **4**, 107133 (2014).
- ⁴⁰ We performed simulations with different in-plane cell size to show that for cells less than about 1.25 nm in-plane, the simulations have converged and do not exhibit errors because of the “staircase” approximation of the rounded edges.
- ⁴¹ J. A. Osborn, *Phys. Rev.* **67**, 351 (1945).
- ⁴² T. Sebastian, K. Schultheiss, B. Obry, B. Hillebrands, and H. Schultheiss, *Frontiers in Physics* **3**, 35 (2015).